

Monte Carlo Simulation of the Crossover from Bose Glass to Bragg Glass Phase in Layered BSCCO with Columnar Defects

L. M. Queiroz and M. D. Coutinho-Filho

Laboratório de Física Teórica e Computacional, Departamento de Física, Universidade Federal de Pernambuco, 50670-901, Recife-PE, Brazil

Monte Carlo simulations of layered BSCCO samples are used to investigate the behavior of vortex matter at low fields, particularly in connection with the possible occurrence of a Bragg glass (BrG) phase at low density of columnar defects, a phenomenon characterized by the prevalence of short-range over long-range order. In this dislocation-free topological phase the translational order correlation function displays a power law decay. For magnetic induction $B = 0.1$ kG the analysis of the data for the first Bragg peak of the planar structure factor, the hexatic order parameter, and the Delaunay triangulation shows that, as the density of columnar defects is lowered, a *crossover* (or transition) from Bose glass to BrG phase takes place in this *highly anisotropic* high- T_c superconductor. Most importantly, an analysis of the 3D vortex-vortex correlation function in terms of the structure factor, calculated via a saddle point approach and the use of the numerical data as input, provides clear-cut evidence of a power law decay of the Bragg peaks in the BrG phase, a fundamental feature that was unequivocally verified only in isotropic compounds.

I. INTRODUCTION

Vortex matter in high- T_c superconductors has been a topic of intensive research^{1–4}. In these systems, the combined effect of magnetic interactions and Josephson coupling between vortices in neighboring planes, thermal agitation, magnetic induction, and disorder, gives rise to very rich phase diagrams. In fact, the understanding of the effects of point disorder and columnar defects has offered a great diversity of experimental and theoretical challenges, particularly those related to the occurrence and properties of glass phases, such as, the vortex glass (VG)^{5,6}, the Bose glass (BG)^{2,7}, and Bragg glass (BrG)^{3,8,9} phases. Most importantly, disorder tends to pin vortices, thus preventing dissipation under an applied electrical current^{1–4,10}, a phenomenon common to type-II superconductors, particularly cuprates under columnar defects: YBCO¹¹, BSCCO¹², and TBCCO¹³; iron-based^{14,15}, and multi-band superconductors in general^{16,17}. Facing these challenges has required high-quality samples with disorder control, and the use of a variety of powerful experimental and theoretical techniques. Pursuing this endeavor, many discoveries and new concepts and mechanisms underlying the related intriguing phenomena have been continued uncovered and put forward. Recent advances include the study of single vortex unzipping (manipulation) using magnetic-force microscopy for extended and point defects^{18,19}, the probe of vortex dynamics and pinning of single vortex in superconductors at nanometer scales²⁰, and relaxation dynamics of vortex lines in disordered type-II superconductors under magnetic field and temperature quenches²¹.

In this work, we focus on cuprate compounds, whose discovery opened the “pandora’s box” thirty years ago: LBCO²², YBCO²³, BSCCO²⁴, and TBCCO²⁵. In clean samples, we highlight the observation of the first-order melting transition of the Abrikosov lattice in BSCCO²⁶

and YBCO²⁷, and its description through the elastic approach²⁸, the so-called boson analogy^{2,29,30} and Monte Carlo (MC) simulations^{1–4}, including the wandering of vortex lines in the solid phase (before melting), and the entanglement, cutting and reconnection of these vortices in the liquid phase (VL). Moreover, these compounds exhibit intermediate or high anisotropy and the phenomenon of decoupling of the CuO₂ layers leading to pancake vortices (point vortices in the 2D CuO₂ layers) at sufficiently high field (magnetic induction)^{31,32}. Despite challenging aspects of the BSCCO $B - T$ phase diagram^{33–35}, the occurrence of vortex matter at intermediate ($0.1 \text{ T} < B < 1 \text{ T}$) and high fields ($1 \text{ T} < B < 10 \text{ T}$), and the decoupling of the CuO₂ planes in high fields at coincidence with the first-order melting transition³⁵, were verified also through Monte Carlo (MC) simulations³⁶ using the Lawrence-Doniach (LD) model³⁷, derived from the anisotropic Landau-Ginzburg model with the neighboring 2D CuO₂ layers coupled via the Josephson interaction.

At this point, we find it is instructive to digress on some fundamental aspects of the BrG, VG, and BG phases, including the contrast and similarities caused by the presence of point disorder or columnar defects. It will prove useful, since our main goal is to study the crossover (or transition) from the BG to the BrG phase, under columnar defects, and to provide clear-cut evidence of diverging Bragg peaks in the BrG phase in highly anisotropic superconductors, such as BSCCO, under low fields and low density of columnar defects. Indeed, this issue remains challenging³, since this fundamental feature was suggested⁹ to explain neutron diffraction data in 2H-NbSe₂³⁸, an isotropic compound, and, most unequivocally, verified³⁹ only on the isotropic single-phase (K, Ba) BiO₃- crystal, under low density of point disorder.

Point Disorder (BrG and VG): In the context of elastic theory the effect of point disorder on the Abrikosov lattice can be classified in three main regimes³. The Larkin-Ovchinnikov regime⁴⁰, in which case the linear coupling of

the displacement field to the disorder causes the breaking of the system into independently pinned domains. The random manifold regime sets in at larger scales⁴¹, with the decay of the translational order correlation function governed by a stretched exponential^{41,42}, instead of the pure exponential decay of the Larkin regime, and verified in dislocation free samples of BSCCO⁴³. Lastly, in the asymptotic regime, displacements grow logarithmic at large scales^{8,9} and the translational order correlation function displays a power law decay. This regime is the so-called BrG phase, a dislocation-free topological phase. Dynamic features of this phase were confirmed in BSCCO⁴⁴, including the moving BrG behavior⁴⁵, both experimentally⁴⁶ and numerically⁴⁷.

In addition, the increase of point disorder or the increase of the magnetic induction B can drive a first-order transition from the low-temperature BrG phase to the VG phase^{5,6,48}, or to a vortex liquid (VL) phase at higher temperatures, as numerically and experimentally verified^{1,3,4}. Indeed, a detailed experimental study of the vortex state in $\text{La}_{1.9}\text{Sr}_{0.1}\text{CuO}_4$ at a macroscopic level reported a change with field from BrG to VG⁴⁹, in which case the microscopic behavior reflects a delicate interplay of thermally induced and pinning-induced disorder. A VG will exhibit off-diagonal long-range order, much in analogy with a spin glass phase, and a single pinned vortex is formally equivalent to a direct polymer in a random media⁶. In fact, as disorder or B increases, dislocations start to proliferate, and the occurrence of a VG phase is experimentally verified by the abrupt change of the Josephson plasma frequency by crossing the BrG-VG first-order transition line (the BrG-VL Transition is also first order)⁵⁰. Notwithstanding, experimental groups have struggled hardly in order to obtain clear-cut $B-T$ phase diagrams⁵¹ in light of the VG and VL phases mentioned above. In particular, an unusual glassy state (pinned vortex liquid) at intermediate fields was recently reported⁵²; in fact, this glass state freezes continuously from the equilibrium VL, but its structure differs from both the low-field BrG and the high-field VG phases.

Columnar defects (BG and BrG): Let us now focus on the effect of columnar or correlated disorder, experimentally motivated by the sizable upward shift of the irreversibility line in heavy-ion irradiated samples of YBCO¹¹, BSCCO¹², and TBCCO¹³. Indeed, an extension of the boson analogy²⁹ allowed the mapping^{2,7} of line vortex under columnar defects onto the problem of two-dimensional disordered driven boson localization⁵³, thereby giving rise to the solid BG phase, the (superfluid) entangled flux liquid phase, and the Mott insulator phase, with one fluxon localized on every pin. It was emphasized⁷ that, despite the similarities of the scaling laws for the BG and VG phases, point disorder promotes wandering and entanglement, while columnar disorder inhibits wandering and promotes localization. Direct contact with experimental observations in BSCCO under columnar defects⁵⁴ was nicely provided^{55,56}, including dynamical effects². In addition, several pertinent

aspects of the distinction between the regimes $B < B_\phi$, where the BG theory fully applies, and the more complex behavior expected for $B > B_\phi$, were reported⁵⁷⁻⁶⁰; here, the matching field is defined by $B = n_d\Phi_0$, where n_d is the disorder concentration and Φ_0 is the superconducting flux quantum. In particular, in contrast to the strong BG regime ($B < B_\phi$), in the weakly pinned BG regime ($B > B_\phi$) the occurrence of an interstitial liquid phase was proposed⁵⁷ to occur between the former phase and the VL phase due to the increase of flux lines and thermal excitations, with the two BG regimes separated by the Mott insulator line at $B = B_\phi$ in a $B-T$ phase diagram. Detailed studies on samples of BSCCO and YBCO with columnar defects were undertaken⁶¹⁻⁶³ in order to clarify the diversity of estimates for the pertinent critical exponents⁶⁴, which contrast with those of the VG transition⁴⁸. In fact, for $B < B_\phi$ the data is well described by the BG theory for vortex pinning and dynamics in the presence of columnar defects, while in the regime $B > B_\phi$ the dynamics is most likely determined by the collective activation of pancake vortices from interstitial vortices not trapped by columnar defects.

Recently⁶⁵, the authors and a collaborator used the LD model to perform MC simulations of 3D layered samples with BSCCO parameters under columnar defects. The numerical data of the temperature behavior of the structure factor and vortex-vortex correlation length along the field (z -direction) brought clear-cut evidence of hysteretic behavior of the vortex matter at intermediate ($0.1 \text{ T} \leq B < 1 \text{ T}$) and high fields ($1 \text{ T} \leq B \leq 10 \text{ T}$), and for $B_\phi/B = 1/4, 1$, and 4 . For this purpose, two representative initial conditions at zero temperature (T) were used: the Abrikosov lattice and a random vortex lattice, mimicking possible configurations in a zero-field-cooled (ZFC) protocol. At intermediate fields and increasing temperature, we observed that both ZFC configurations evolve through metastable states and meet the pristine melting transition line $B_m(T)$, thus defining the melting temperature T_m for a given B . We also verified that, in both cases, the vortex matter undergoes a smooth plane decoupling transition (formation of pancake-like vortex structure) around T_m , with the correlation length along the z -direction characterized by a T -dependent exponential decay with z . In this regime, we can also visualize vortex pinning to one or two neighboring columnar defects at the onset of vortex depinning, and entanglement between two vortices above melting. In addition, the very relevant case of the field-cooling (FC) process from an initial temperature $T_0 = 79 \text{ K}$ at the VL phase is also considered. In this case, as T decreases under intermediate field values, the system evolves through metastable states of an inhomogeneous phase of unpinned vortices coexisting with pinned ones (BG background). Lastly, the system reaches a FC robust BG phase down to very low T . We stress that, under the above-mentioned conditions, the melting and decoupling scenario for the ZFC and FC protocols are practically identical. On the other hand, for high fields and under the ZFC proto-

cols, the melting transition is practically concurrent with the discontinuous decoupling of the CuO₂ planes; while, under FC, the vortex lattice decouples at a temperature below the melting transition. Indeed, under FC, we identify that the exchange between flux lines is the underlying mechanism for plane decoupling and the formation of a pancake-like vortex structure.

At this stage, it is worth mentioning that the corresponding melting and BG lines at intermediate and high fields mentioned above⁶⁵ can be incorporated quite successfully in the B-T phase diagram of BSCCO samples^{33,35}. They are also compatible with phase diagrams (pin concentration versus temperature) derived using numerical functional minimization techniques of electromagnetic interactions between vortices^{66–68} and MC simulations of the 3D frustrated anisotropic XY model⁶⁹ (see phase diagrams in Figs. 1 of both references 67 and 69), apart from details inherent to the use of distinct approaches and choice of parameters. Moreover, MC simulations using the LD model for BSCCO at $B = 125$ G, and $B_\phi/B = 1/5$,⁷⁰ found that the vortex matter displays an increase of the magnitude of the structure factor at the first Bragg peak and of the line wandering along the z direction, just before the transition to the IL phase, consistent with our results at intermediate fields⁶⁵.

We also remark that the melting scenario at low-fields observed in BSCCO for $B \leq 200$ G and 5 G $\leq B_\phi \leq 100$ G⁷¹, including dynamical effects and oblique fields⁷², have also identified an intermediate phase which resembles the one found in Ref. 65 at intermediate and high fields. Indeed, the low-field scenario evidences that the delocalization (or depinning) line, separates the homogeneous VL phase from an inhomogeneous one in which nanodroplets of vortex liquid are caged in the pores of a solid skeleton formed by vortices pinned on columnar defects (porous vortex matter). It is also verified that all pertinent lines merge to the low-field pristine melting line $B_m^0(T)$, which ends at $B_m^0(T_c) = 0$. This scenario is also consistent with analytical⁷³ and appropriate numerical modeling⁷⁴. The above features are very important in the context of identifying the nature of phases in the $B - T$ phase diagram of BSCCO, as discussed for clean samples³⁶ in the second paragraph of this section, and extended in Ref. 65, and in this manuscript, to include the effect of columnar disorder.

In the next sections we shall our numerical and analytic studies with focus on the main goals of our work, namely, the numerical-analytic description of the crossover (or transition) from the BG to the BrG phase, under columnar defects, and the clear-cut evidence of diverging Bragg peaks in the BrG phase in a highly anisotropic superconductor with BSCCO parameters, under low fields and low density of columnar defects. In Sec. II we describe the LD model, suitable to describe highly anisotropic BSCCO samples, the phenomenological physical quantities, and the simulation procedure. In Sec. III we present the results related to both hexatic order parameter and the first Bragg peak of the structure factor for

the vortex matter at different disorder concentrations, supplemented by the Delaunay triangulation of the vortices. Quite rewarding, we find that, at $B = 100$ G and $B = B/32$, the in-plane structure factor displays sharp Bragg peaks hexagonally distributed on the lattice; in fact, we observe that the system undergoes a crossover from a BG to a BrG phase as B is lowered from $B_\phi = B$ to $B_\phi = B/32$. In Sec. IV we examine the 3D vortex-vortex correlation function in terms of its Fourier transform, i. e., the 3D structure factor. A saddle point calculation, and the use of the numerical data as input, clearly demonstrates the occurrence of divergent Bragg peaks for simulated BSCCO samples in a BrG phase under low fields and low density of columnar defects. Lastly, Sec. V is devoted to our concluding remarks.

II. MODELING BSCCO WITH COLUMNAR DEFECTS

We consider that the flux lines in a layered superconductor is an array of point-like pancake vortices bound together by an interlayer Josephson interaction^{36,37,75}. We perform Metropolis MC simulations on a system with 64 vortex lines on a grid of $256 \times 222 \times N_z$, with $N_z = 64$ layers and periodic boundary conditions in all directions. We use 10^5 MC steps for each temperature, with $\Delta T = \pm 1$ K, and discard the first 2×10^4 ones in the averaging process. We choose the following parameters, adequate for BSCCO¹: $d = 15$ Å, $s = 1.66$ Å, $\lambda_0 = 1414.2$ Å, $T_c = 87$ K, $\xi_{ab}(0) = 21$ Å, $\gamma = 100$, where d is the interlayer spacing, s is the thickness of a layer, λ_0 is the penetration depth at $T = 0$, such that $\lambda_{ab}(T) = \lambda_0(1 - T/T_c)^{-1/2}$, $\xi_{ab}(0)$, is the coherence length in the ab plane at $T = 0$, where T_c is the the zero-field critical temperature, and $\gamma = \lambda_z/\lambda_{ab} = \sqrt{2}\xi_{ab}(0)/(\sqrt{g}d)$ measures the ratio between axial and planar penetration depths, where g is the interlayer Josephson coupling strength.

We use the Lawrence-Doniach model, in which the system is represented by a stack of superconducting planes. Each plane has a certain number of interacting vortices, whose free energy is given by^{36,37,75}

$$F_{LD} = \frac{1}{8\pi} \int d^3r \mathbf{B}^2(r) + \frac{dH_c^2}{8\pi} \sum_{z=1}^{L_z} \int d^2\rho \left\{ \left(1 - \frac{T}{T_c}\right) |\psi_z|^2 + \frac{1}{2} \beta |\psi_z|^4 + |\xi_{ab}(T)(\nabla_{ab} - 2ie\mathbf{A}_{ab})\psi_z|^2 - g \left| \exp \left(2ie \int_{z+d}^z dz A_z \right) \psi_{z+d} - \psi_z \right|^2 \right\}, \quad (1)$$

where $\mathbf{B}(r)$ is the local magnetic induction, ψ_z denotes the dimensionless superconducting order parameter, $H_c(T)$ is the thermodynamic critical magnetic field, e is the electron charge, β is the Landau coefficient of the quartic term in $|\psi_z|$, ∇_{ab} is the in-plane gradient, \mathbf{A}_{ab} (A_z) is the vector potential in the ab plane (at the layer z). ρ is a position in the ab plane. The above Helmholtz

free energy is considered instead of the Gibbs one, since in our simulations we consider fixed B (constant number of vortices) along the z axis perpendicular to the superconducting ab planes. It is worth mentioning that the conditions for a smooth connection⁷⁶ between the LD model and the anisotropic Ginzburg-Landau model was properly discussed in Ref. 77, where rigorous aspects of the procedure were put forward.

Since our study is done in terms of a vortex representation, one can minimize Eq. (1) to obtain the various contributions to the energy of the system. Taking the London limit ($|\psi_z|$ constant throughout the sample), the Josephson interaction between a pair of adjacent layers can be expressed as^{1,37,78}

$$V_J = \frac{\Phi_0^2}{16\pi^3 \lambda_{ab}^2 \gamma^2 d} \int d^2 \rho [1 - \cos(\tilde{\varphi}_{z+d} - \tilde{\varphi}_z)], \quad (2)$$

where $\tilde{\varphi}_z$ is the gauge-invariant phase of ψ_z . The difference $\tilde{\varphi}_{z+d} - \tilde{\varphi}_z$ can be calculated for the case of one single pancake vortex dislocated from the flux line by a minimization procedure of Eq. (1). This leads to

$$\nabla_{ab}^2(\tilde{\varphi}_{z+d} - \tilde{\varphi}_z) = \left(\frac{1}{\gamma^2 d^2} + \frac{1}{\lambda_z^2} \right) \sin(\tilde{\varphi}_{z+d} - \tilde{\varphi}_z). \quad (3)$$

Considering $\lambda_z \gg \gamma d$, one can solve Eq. (3) and calculate the Josephson energy V_J . We define $\rho_i(z)$ as the 2D vector position of the pancake vortex belonging to the i -th flux line at plane z . For vortices whose planar distance $r_1 = |\rho_i(z+d) - \rho_i(z)|$ is much less than the length scale γd , $V_J \sim (r_1/\gamma d)^2 \ln(\gamma d/r_1)$. For $r_1 \gg \gamma d$, the dependence of V_J on r_1 is linear. Therefore, in our calculations, we have used the following expression for V_J :

$$\begin{aligned} & \frac{d\Phi_0^2}{8\pi^3 \lambda_{ab}^2} \left[1 + \ln\left(\frac{\lambda_{ab}}{d}\right) \right] \frac{r_1^2}{(\gamma d)^2} \ln\left(\frac{\gamma d}{r_1}\right), \text{ if } r_1 \leq \gamma d; \\ & \frac{d\Phi_0^2}{8\pi^3 \lambda_{ab}^2} \left[1 + \ln\left(\frac{\lambda_{ab}}{d}\right) \right] \left(\frac{r_1}{(\gamma d)} - 1 \right), \text{ otherwise.} \end{aligned} \quad (4)$$

For vortices on the same plane, the magnetic repulsion can be given by the 2D Ginzburg-Landau model^{1,37}:

$$V_{plane} = \frac{\Phi_0^2 s}{8\pi^2 \lambda_{ab}^2} K_0\left(\frac{|\rho_{ij}(z)|}{\lambda_{ab}}\right), \quad (5)$$

where $\rho_{ij} = |\rho_i(z) - \rho_j(z)|$.

We also introduce columnar randomly distributed defects on the sample, with the local disorder potential V_D defined by the correlator:

$$\overline{V_D(\rho)V_D(\rho')} = E_p \delta_2(\rho - \rho'), \quad (6)$$

where $\delta_2(\rho)$ is the 2D Dirac delta function, $E_p = -100$ K, in units of the Boltzmann constant k_B , is the pinning energy, and the bar represents the disorder average. The energy to be minimized following the MC procedure

discussed above reads:

$$\begin{aligned} E = & \sum_{i,z} V_D(\rho_i(z)) + \sum_{i,z} V_J(|\rho_i(z+d) - \rho_i(z)|) \\ & + \frac{1}{2} \sum_{i,j,z} V_{plane}(|\rho_i(z) - \rho_j(z)|). \end{aligned} \quad (7)$$

Our approach allows us to calculate the first Bragg peak of the in-plane structure factor, $S(k_{\text{Bragg}})$, where $S(\mathbf{k}_\perp) = S(\mathbf{k}_\perp, z=0)$ is the planar structure factor in the momentum space $\mathbf{k}_\perp = (k_x, k_y)$, and

$$S(\mathbf{k}_\perp, z) = \left[\frac{1}{\Omega N} \sum_{\rho} \langle n(0,0)n(\rho, z) \rangle e^{i\mathbf{k}_\perp \cdot \rho} \right]_{av}, \quad (8)$$

where $\langle n(0,0)n(\rho, z) \rangle$ is the density-density correlation function in plane z , N is the number of lines, Ω is a normalization constant such that, for an Abrikosov lattice, $S(k_{\text{Bragg}}) = 1$, $n(\rho, z)$ is the density of vortices at position (ρ, z) , $\langle \dots \rangle$ denotes the thermal average, whereas $[\dots]_{av}$ stands for the process of sampling disorder average. Most importantly, we have also calculated the hexatic order parameter,

$$\Psi_6 = \sum_{i=1}^N \frac{1}{z_i} \sum_{j=1}^6 e^{6i\theta_{ij}}, \quad (9)$$

where θ is the bond angle between next-neighbor vortices, and z_i is the number of next-neighbors in the i th plane. Note that, for the hexagonal lattice, $\Psi_6 = 1$. Other pertinent correlation functions, including the root mean square deviation of vortices along the z direction, whose connection with the 3D vortex-vortex correlation function and the structure factor is provided in Section IV and allows us to show that identified BrG phase indeed exhibits divergent Bragg peaks, have also been calculated.

III. HYSTERETIC BEHAVIOR AND CROSSOVER FROM BG TO BRG PHASE

We have measured the structure factor and the hexatic order parameter of samples under $B = 0.1$ kG and $B_\phi = B$, $B_\phi = B/8$, and $B_\phi = B/32$. We averaged these quantities over 30 samples for three initial conditions at $T = T_0$: Abrikosov and random lattices, both at $T_0 = 0$ with T increasing to a $T_{\text{final}} = 0$ above melting; and a field-cooling (FC) protocol with $T_0 = 80$ K (above melting) with T lowering down to $T_{\text{final}} = 0$.

Figure 1 displays the first Bragg peak of the structure factor $S(k_{\text{Bragg}})$ [Figs. 1(a), 1(c), and 1(e)] and the hexatic order parameter Ψ_6 [Figs. 1(b), 1(d), and 1(f)].

Figures 1(a) and 1(b) exhibit $S(k_{\text{Bragg}})$ and Ψ_6 , respectively, at the doping $B_\phi = B$. In Fig. 1(a), for both Abrikosov and random initial lattice configurations, we can notice a distinct behavior in comparison with the

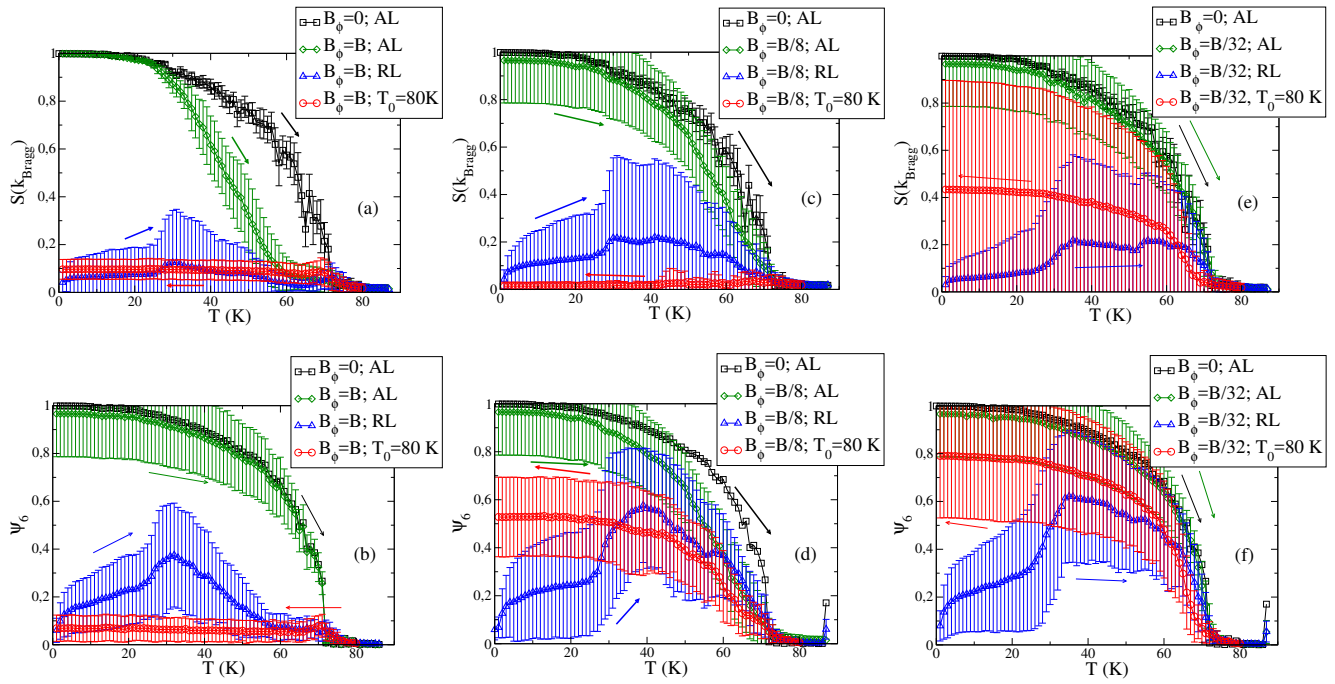


FIG. 1. (Color online) First Bragg peak of the structure factor $S(k_{\text{Bragg}})$ [(a), (c) and (e)] and hexatic order parameter [(b), (d) and (f)], as a function of temperature for $B = 0.1$ kG and $B_\phi = B$ [(a) and (b)], $B_\phi = B/8$ [(c) and (d)] and $B_\phi = B/32$ [(e) and (f)]. Data from pristine samples ($B_\phi = 0$) are shown for comparison, including sampling fluctuations. For $B_\phi \neq 0$ and distinct boundary conditions: Abrikosov lattice (AL), random lattice (RL), and field cooling with $T_0 = 8$ K; the sampling disorder average are indicated by a darker color curve (green, blue, and red). The arrows indicate data for increasing or decreasing temperature.

data for strong and intermediate fields⁶⁵. Indeed, in the present case $S(k_{\text{Bragg}})$ intersects the curve for the pristine sample only at the melting transition (within error bars). As for the FC protocol, we see that, after cooling below the melting temperature, the system settles itself in a glassy configuration and remains there down to $T = 0$. We identify this vortex “freezing” with the BG phase also observed in higher fields⁶⁵, although here we find a smaller magnitude for the first Bragg peak, i.e., $S(k_{\text{Bragg}}) \simeq 0.1$. Now, observing Fig. 1(b), we note that, for both Abrikosov and random initial conditions, the average value and error bars of Ψ_6 are larger than those associated with $S(k_{\text{Bragg}})$ in Fig. 1(a). However, under the FC protocol, $S(k_{\text{Bragg}})$ is slightly more robust than Ψ_6 , which exhibits larger error bars. This signals the onset of the BrG-BG crossover.

Figures 1(c) and 1(d) display $S(k_{\text{Bragg}})$ and Ψ_6 for $B_\phi = B/8$, respectively, for the same families of initial configurations analyzed in the case $B_\phi = B$. Figure 1(c) shows that, for the Abrikosov initial configuration, $S(k_{\text{Bragg}})$ is close to the pristine case (within error bars). In the case of random initial configuration, $S(k_{\text{Bragg}})$ exhibits a rather steep increase with temperature and meets the Abrikosov lattice at melting. However, under the FC protocol, the system settles itself in a configuration such that $S(k_{\text{Bragg}})$ is practically zero. On the contrary, Fig. 1(d) shows that, under the FC protocol, the average of Ψ_6

stabilizes well above zero, which signals that the local order is preserved, and the BrG phase sets in for this value of B_ϕ . Figure 1(d) also shows that, for the Abrikosov initial configuration, the behavior of the average of Ψ_6 is quite similar to that of $S(k_{\text{Bragg}})$ in Fig. 1(c). In addition, for the random initial configuration, it exhibits a high peak at $T \simeq 40$ K and meets the Abrikosov curve from $T \simeq 60$ K onwards.

Lastly, Figs. 1(e) and 1(f) present $S(k_{\text{Bragg}})$ and Ψ_6 , respectively, for $B_\phi = B/32$, a very low concentration of defects. Figure 1(e) shows that, for the Abrikosov initial configuration, the low concentration of defects does not affect much the T -dependence of $S(k_{\text{Bragg}})$ relative to Fig. 1(c). Further, the data of $S(k_{\text{Bragg}})$ for the random initial configuration is similar to that of Fig. 1(c). However, the most salient feature of Fig. 1(e) is the large error bars of the data of $S(k_{\text{Bragg}})$ under the FC protocol. It is so because, in this case, there are two distinct families of metastable glassy configurations: one in which $S(k_{\text{Bragg}})$ is close to zero; and the other in which $S(k_{\text{Bragg}})$ is close to the pristine curve. Both families seem equally probable from a stability viewpoint. On the other hand, Fig. 1(f) shows that there is no significant difference between Ψ_6 using the Abrikosov initial configuration and a pristine sample. Likewise, for the random initial configuration, Ψ_6 here is similar to that of Fig. 1(e). However, the most evident difference in the

behavior of $S(k_{\text{Bragg}})$ and Ψ_6 under the FC protocol is that the average of Ψ_6 is robust and remains closer to the pristine curve.

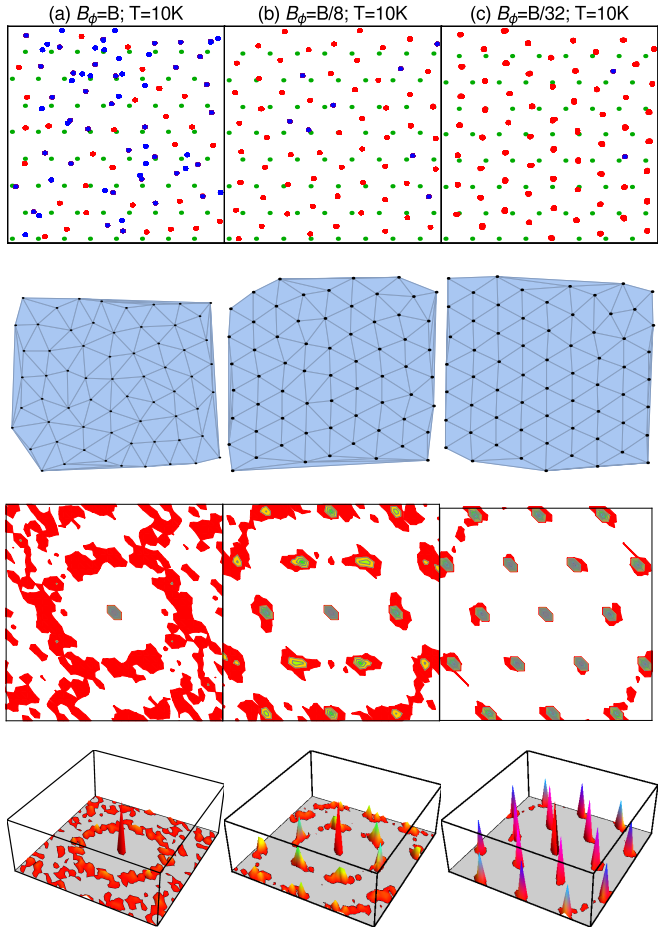


FIG. 2. (Color online) Planar projection of a typical vortex lattice configuration, columnar defects and Abrikosov lattice, indicated in the first row by red, blue, and green dots, respectively for $B = 0.1$ kG at $T = 10$ K for FC samples starting at $T_0 = 80$ K. The second row displays Delaunay triangulation of the planar projection of the vortex lattice. Third row exhibits the planar structure factor $S(k_x, k_y)$ of the vortex lattice. Data were obtained from sample with (a) $B_\phi = B$ (first column), (b) $B_\phi = B/8$ (second column), and (c) $B_\phi = B/32$ (third column).

In order to unveil the effect of the presence of short or long range order on FC samples under lower doping, we must observe the actual configuration of vortices. In this context, the first row of Fig. 2 exhibits the vortex configurations at $T = 10$ K for $B_\phi = B$ [Fig. 2(a)], $B_\phi = B/8$ [Fig. 2(b)], and $B_\phi = B/32$ [Fig. 2(c)], respectively.

In Fig. 2(a), we observe that the lattice is indeed disordered, with many vortices (in red) pinned to the defects (in blue), making the configuration diverge from the ideal Abrikosov lattice (in green). This can be corroborated by

the Delaunay triangulation in the first diagram of the second row, which suggests the occurrence of many vortices with coordination number equal to five or seven, instead of six. In the third row, the Fig. shows that the system does not have sharp Bragg peaks at this temperature, but rather displays the characteristics of a BG phase.

Figure 2(b) shows that, for $B_\phi = B/8$, though some vortices are pinned, the system resembles a reoriented hexagonal lattice. In the second diagram of the second row, we observe some distortions relative to the ideal hexagonal lattice. There are some vortices with coordination number different from six, although they are relatively isolated within the lattice. In the last row the structure factor, featuring six Bragg peaks, is displayed. This is an evidence that we have reached, within numerical precision, the onset of the BrG phase.

The first row of Fig. 2(c) shows that the vortices, for $B_\phi = B/32$, are almost in an hexagonal lattice. As our simulations use 64 vortices, $B_\phi = B/32$ means there are only two defects in the system. These two defects have the effect of making the lattice to reorient itself, but not losing its approximately hexagonal character, besides some few distortions that can be better viewed in the Delaunay triangulation of the second row of this column. These distortions, as expected, occur close to one of the defects and are localized, not spreading to other sites of the lattice. In the last row, we see the structure factor exhibiting sharp secondary Bragg peaks whose positions are in a hexagonal structure, which clearly indicates that this phase is a BrG phase.

In short, Fig. 2 strongly evidences the already mentioned crossover from a BG to a BrG phase as B_ϕ is lowered, in which case Figs. 2(k) and 2(l) display the Bragg peaks around the central peak for $B_\phi = B/8$ and $B_\phi = B/32$, respectively.

IV. BRG PHASE AND DIVERGENT BRAGG PEAKS

The results of the previous section gave us evidence of the presence of a BrG phase in our simulations. Nonetheless, to confirm it, we must verify that the structure factor diverges algebraically as the wave vector $k \rightarrow 0$, or, equivalently, that the correlation function decreases more slowly than a standard exponential decay at large distances. However, since our system has a finite size, it imposes us a limitation: the wave vector resolution is limited to $\Delta k = 2\pi/L$, where L is the size of the system. Here, we use an approach compatible with that of Giarmarichi and Le Doussal⁹, and also employed by Klein *et al.*³⁹ to identify the BrG phase from neutron diffraction data from a *isotropic* single-phase (K, Ba)BiO₃ crystal at $T = 2$ K. In fact, the experimentally observed lorentzian behavior of the structure factor observed for various field values implies a decrease of the central peak with increasing field, while the width of the curve does not change. Instead, in our numerical-analytical description, the field

and temperature are fixed, while the density of columnar defects decreases, and the numerical data is used as input. The width of the lorentzian curve is in fact limited by the experimental resolution or by the numerical accuracy.

Let $\mathbf{r}(z) = (x(z), y(z))$ be the position of a given vortex in the z layer. We define the root mean square deviation of the position of the vortices along the z -direction as

$$\Delta r_{rms}^2(|z - z'|) = \overline{\langle |\mathbf{r}(z) - \mathbf{r}(z')|^2 \rangle}, \quad (10)$$

where the angular bracket represents the Boltzmann thermal average and the upper bar the disorder average. On the other hand, we define the 3D vortex-vortex correlation function G in terms of its Fourier transform, i. e., the 3D structure factor $S(\mathbf{k})$:

$$G(|\mathbf{r} - \mathbf{r}'|) = \frac{V}{N} \int S(\mathbf{k}) e^{-i\mathbf{k}_\perp \cdot (\mathbf{r} - \mathbf{r}')} e^{-ik_z(z - z')} d^3k, \quad (11)$$

where V is the volume of the system, and N is the total number of vortices. We can estimate the spatial dependence of G by taking the saddle point of Eq. (11) around the Bragg peaks and under disorder average. We thus retain only the Bragg peaks average:

$$G(|\mathbf{r} - \mathbf{r}'|) \simeq \frac{8\pi^3}{N} \sum_{\mathbf{K}} S(\mathbf{K}) \overline{\langle e^{-i\mathbf{K}_\perp \cdot (\mathbf{r} - \mathbf{r}')} \rangle}. \quad (12)$$

Note that (12) has no explicit dependence on z ; indeed, since the z -component of the Bragg vector $K_z = 2\pi m/d$ and $z - z' = nd$, where n and m are integers, $e^{iK_z(z - z')} = 1$. In addition, the right hand side of (12) must be real, thereby

$$G(|\mathbf{r} - \mathbf{r}'|) \simeq \frac{8\pi^3}{N} \sum_{\mathbf{K}} 2S(\mathbf{K}) \overline{\langle \cos(\mathbf{K}_\perp \cdot (\mathbf{r} - \mathbf{r}')) \rangle}; \quad (13)$$

and at low temperatures, we can safely write:

$$G(|\mathbf{r} - \mathbf{r}'|) \simeq \frac{8\pi^3}{N} \sum_{\mathbf{K}} 2S(\mathbf{K}) \overline{\left\langle 1 - \frac{K_\perp^2}{2} |\mathbf{r}(z) - \mathbf{r}(z')|^2 \right\rangle}, \quad (14)$$

which implies

$$G(|\mathbf{r} - \mathbf{r}'|) \simeq C_1 - C_2 \Delta r_{rms}^2(|z - z'|), \quad (15)$$

where C_1 and C_2 are constants.

The results above show that we can use the root mean square deviation of the position of the vortices in order to estimate the decay of their correlation function along the z direction. We thus retrieve the dependence of the structure factor on k_z , through the following Fourier transform:

$$\sigma(k_z) = \left| \int \Delta r_{rms}^2 e^{ik_z(z - z')} d(z - z') \right|. \quad (16)$$

As the planes are discretized, with a distance d between each other, the integral of (16) can be transformed into a sum over all planes of the sample:

$$\sigma(k_z) = \left| \sum \Delta r_{rms}^2 e^{ink_z d} \right|. \quad (17)$$

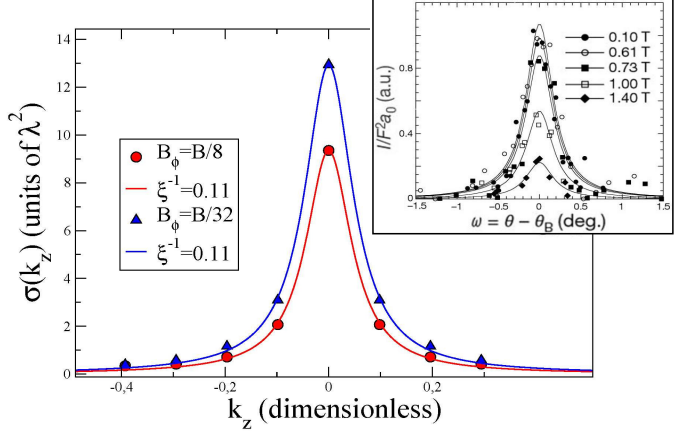


FIG. 3. (Color online) $\sigma(k_z)$, defined by Eq. 17, for a sample at $T = 10$ K for $B = 0.1$ kG with $B_\phi = B/8$ (red dots) and $B_\phi = B/32$ (blue triangles). The curves represent lorentzian fits for each data set. Both fits have width $\xi^{-1} \simeq 0.11$, very close to the numerical resolution $\Delta k_z = 2\pi/64 \simeq 0.1$. For comparison, the inset shows experimental data of the neutron beam intensity diffracted by vortices in a single-phase (K, Ba)BiO₃ crystal taken from Ref. 39.

We have calculated Δr_{rms}^2 for samples at $T = 10$ K, averaged over columnar disorder, and $B_\phi = B/8$ and $B_\phi = B/32$. We have also calculated the discrete Fourier transform $\sigma(k_z)$ of Δr_{rms}^2 and fitted the data to a lorentzian, in the context of the Ornstein-Zernike framework⁷⁹:

$$\sigma(k_z) = \frac{A}{(\xi^{-1}/2)^2 + k_z^2}, \quad (18)$$

where ξ^{-1} is the width of the lorentzian. As $N_z \rightarrow \infty$, $\xi^{-1} \rightarrow 0$ and $\sigma(k_z) \sim k_z^{-2}$, which characterizes an algebraic divergence at $k_z = 0$. However, our minimum fitting value of ξ^{-1} is limited by the numerical precision $\Delta k_z = 2\pi/N_z = 2\pi/64$. Figure 3 displays the results of $\sigma(k_z)$ for the two distinct averaged samples. Although the peaks have different heights, the width of the lorentzian fit is the same, a signature of a BrG phase. In fact, the fitting value for the two samples is $\xi^{-1} \simeq 0.11$, which is very close to the numerical resolution. We believe this is a conclusive evidence of the emergence of the BrG phase in our simulations at low fields and low columnar disorder with BSCCO parameters. For comparison, the inset in Fig. 3 shows the experimental data³⁹ of the neutron beam intensity I diffracted by vortices in the isotropic single-phase (K, Ba)BiO₃ crystal, where F is the single-vortex standard form factor, a_0 is the lattice

spacing, and $\omega = \theta - \theta_B$ measures the mismatch of the angle θ , where θ is the angle between the magnetic field and the neutron beam, and θ_B is the Bragg angle.

V. CONCLUDING REMARKS

In this work, we presented simulations of *highly anisotropic* layered samples with BSCCO parameters, in the low field regime with focus on the observation of the crossover from BG to BrG phase as the density of columnar defects is lowered.

Under the above conditions, the vortices tend to stay in a glassy phase with sharp Bragg peaks. In particular, using the field-cooling protocol, we verified that the hexatic order parameter Ψ_6 is far greater than $S(k_{\text{Bragg}})$, which implies the prevalence of short range over long range order.

Notably, by examining the behavior of the 3D structure factor along the z direction by means of a relation between the vortex-vortex correlation function and the root mean square deviation of the positions of the vortices, we found that it fits to a lorentzian function close to $k_z = 0$, with the same width for the simulated samples. -This feature is a signature of the occurrence of a BrG phase under low fields and low densities of columnar defects, and provides a clear-cut demonstration of the algebraic divergence of the Bragg peaks as the wave vector along the field direction $k_z \rightarrow 0$, in the context of Ornstein-Zernike framework.

ACKNOWLEDGMENTS

This work was supported by CNPq and FACEPE through the PRONEX program, and CAPES (Brazilian agencies).

¹ G. Blatter, M. V. Feigel'man, V. B. Geshkenbein, A. I. Larkin, and V. M. Vinokur, *Rev. Mod. Phys.* **66**, 1125 (1994).

² D. R. Nelson, *Defects and Geometry in Condensed Matter Physics* (Cambridge University Press, Cambridge, 2002).

³ P. Le Doussal, *Int. J. Mod. Phys.* **24**, 3855 (2010).

⁴ B. Rosenstein and D. Li, *Rev. Mod. Phys.* **82**, 109 (2010).

⁵ M. P. A. Fisher, *Phys. Rev. Lett.* **62**, 1415 (1989).

⁶ D. S. Fisher, M. P. A. Fisher, and D. A. Huse, *Phys. Rev. B* **43**, 130 (1991).

⁷ D. R. Nelson and V. M. Vinokur, *Phys. Rev. Lett.* **68**, 2398 (1992); *Phys. Rev. B* **48**, 13060 (1993).

⁸ T. Nattermann, *Phys. Rev. Lett.* **64**, 2454 (1990).

⁹ T. Giamarchi and P. Le Doussal, *Phys. Rev. Lett.* **72**, 1530 (1994); *Phys. Rev. B* **52**, 1242 (1995).

¹⁰ J. Bardeen and M. J. Stephen, *Phys. Rev.* **140**, A1197 (1965).

¹¹ L. Civale, A. D. Marwick, T. K. Worthington, M. A. Kirk, J. R. Thompson, L. Krusin-Elbaum, Y. Sun, J. R. Clem, and F. Holtzberg, *Phys. Rev. Lett.* **67**, 648 (1991); M. Konczykowski, F. Rullier-Albenque, E. R. Yacoby, A. Shaulov, Y. Yeshurun, and P. Lejay, *Phys. Rev. B* **44**, 7167 (1991).

¹² W. Gerhäuser, G. Ries, H. W. Neumüller, W. Schmidt, O. Eibl, Saemann-Ischenko, and S. Klaumünzer, *Phys. Rev. Lett.* **68**, 879 (1992); J. R. Thompson, Y. R. Sun, H. R. Kerchner, D. K. Christen, B. C. Sales, B. C. Chakoumakos, A. D. Marwick, L. Civale, and J. O. Thomson, *Appl. Phys. Lett.* **60**, 2306 (1992).

¹³ R. C. Budhani, M. Suenaga, and S. H. Liou, *Phys. Rev. Lett.* **69**, 3816 (1992).

¹⁴ A. A. Kordyuk, *Low Temp. Phys.* **38**, 888 (2012).

¹⁵ H. Hosono, K. Tanabe, E. Takayama-Muromachi, H. Kageyama, S. Yamanaka, H. Kumakura, M. Nohara, H. Hiramatsu, and S. Fujitsu, *Sci. Tech. Adv. Mat.* **16**, 033503 (2015).

¹⁶ J. A. Drocco, C. J. O. Reichhardt, C. Reichhardt, and A. R. Bishop, *J. Phys.: Cond. Matt.* **25**, 345703 (2013).

¹⁷ X. B. Xu, H. Fangohr, M. Gu, W. Chen, Z. H. Wang, F. Zhou, D. Q. Shi, and S. X. Dou, *J. Phys.: Cond. Matt.* **26**, 115702 (2014).

¹⁸ Y. Kafri, D. R. Nelson, and A. Polkovnikov, *Phys. Rev. B* **76**, 144501 (2007).

¹⁹ O. M. Auslaender, L. Luan, E. W. Straver, J. E. Hoffman, N. C. Koshnick, E. Zeldov, D. A. Bonn, R. Liang, W. N. Hardy, and K. A. Moler, *Nature Phys.* **5**, 35 (2009).

²⁰ L. Embo et al., *Sci. Rep.* **5**, 7598 (2015).

²¹ H. Assi, H. Chaturvedi, U. Dobramysl, M. Pleimling, and U. C. Täuber, *Phys. Rev. E* **92**, 052124 (2015).

²² J. Bednorz and K. Müller, *Z. Phys. B* **64**, 189 (1986).

²³ M. K. Wu, J. R. Ashburn, C. J. Torng, P. H. Hor, R. L. Meng, L. Gao, Z. J. Huang, Y. Q. Wang, and C. W. Chu, *Phys. Rev. Lett.* **58**, 908 (1987).

²⁴ H. Maeda, Y. Tanaka, M. Fukutomi, and T. Asano, *Jap. J. Appl. Phys.* **27**, L209 (1988); M. A. subramanian, C. C. Torardi, J. C. Calabrese, J. Gopalakrishnan, K. J. Morrissey, T. R. Askew, R. B. Flippin, U. Chowdry, and A. W. Sleight, *Science* **239**, 1015 (1988).

²⁵ Z. Z. Sheng, A. M. Hermann, A. El Ali, C. Almasan, J. Estrada, T. Datta, and R. J. Matson, *Phys. Rev. Lett.* **60**, 937 (1988); Z. Z. Sheng and A. M. Hermann, *Nature (London)* **332**, 138 (1988).

²⁶ E. Zeldov, D. Majer, M. Konczykowski, V. B. Geshkenbein, V. M. Vinokur, and H. Shtrikman, *Nature (London)* **375**, 373 (1995).

²⁷ A. Schilling, R. Fisher, N. Phillips, U. Welp, D. Dasgupta, W. Kwok, and G. Crabtree, *Nature* **382**, 791 (1996); A. Schilling, R. A. Fisher, N. E. Phillips, U. Welp, W. K. Kwok, and G. W. Crabtree, *Phys. Rev. Lett.* **78**, 4833 (1997).

²⁸ E. H. Brandt, *Rep. Prog. Phys.* **58**, 1465 (1995).

²⁹ D. R. Nelson, *Phys. Rev. Lett.* **60**, 1973 (1988); D. R. Nelson and H. S. Seung, *Phys. Rev. B* **39**, 9153 (1989).

³⁰ H. Nordborg and G. Blatter, *Phys. Rev. Lett.* **79**, 1925 (1997).

³¹ A. Schilling, R. Jin, J. D. Guo, and H. R. Ott, *Phys. Rev. Lett.* **71**, 1899 (1993).

³² A. E. Koshelev, *Phys. Rev. Lett.* **77**, 3901 (1996); *Phys. Rev. B* **56**, 11201 (1997).

³³ D. T. Fuchs, E. Zeldov, T. Tamegai, S. Ooi, M. Rappaport, and H. Shtrikman, *Phys. Rev. Lett.* **80**, 4971 (1998); T. Shibauchi, T. Nakano, M. Sato, T. Kisu, N. Kameda, N. Okuda, S. Ooi, and T. Tamegai, *Phys. Rev. Lett.* **83**, 1010 (1999).

³⁴ Y. Ando and K. Nakamura, *Phys. Rev. B* **59**, R11661 (1999).

³⁵ J. Torres, R. R. da Silva, S. Moehlecke, and Y. Kopelevich, *Solid State Comm.* **125**, 11 (2003).

³⁶ L. P. Viana, E. P. Raposo, and M. D. Coutinho-Filho, *Phys. Rev. B* **70**, 134516 (2004), and references therein.

³⁷ S. Ryu, S. Doniach, G. Deutscher, and A. Kapitulnik, *Phys. Rev. Lett.* **68**, 710 (1992); M. Hellerqvist, S. Ryu, L. Lombardo, and A. Kapitulnik, *Physica C* **230**, 170 (1994).

³⁸ U. Yaron, P. L. Gammel, D. A. Huse, R. N. Kleiman, C. S. Oglesby, E. Bucher, B. Batlogg, D. J. Bishop, K. Mortensen, K. Clausen, C. A. Bolle, and F. De La Cruz, *Phys. Rev. Lett.* **73**, 2748 (1994).

³⁹ T. Klein, I. Joumard, S. Blanchard, J. Marcus, R. Cubitt, T. Giamarchi, and P. Le Doussal, *Nature (London)* **413**, 404 (2001).

⁴⁰ A. Larkin, Sov. Phys. JETP **31**, 784 (1970); A. I. Larkin and Y. N. Ovchinnikov, *J. Low Temp. Phys.* **34**, 409 (1979).

⁴¹ M. V. Feigel'man, V. B. Geshkenbein, A. I. Larkin, and V. M. Vinokur, *Phys. Rev. Lett.* **63**, 2303 (1989).

⁴² J.-P. Bouchaud, M. Mézard, and J. S. Yedidia, *Phys. Rev. Lett.* **67**, 3840 (1991); *Phys. Rev. B* **46**, 14686 (1992).

⁴³ P. Kim, Z. Yao, C. A. Bolle, and C. M. Lieber, *Phys. Rev. B* **60**, R12589 (1999).

⁴⁴ D. T. Fuchs, R. A. Doyle, E. Zeldov, S. F. W. R. Rycroft, T. Tamegai, S. Ooi, M. L. Rappaport, and Y. Myasoedov, *Phys. Rev. Lett.* **81**, 3944 (1998).

⁴⁵ T. Giamarchi and P. Le Doussal, *Phys. Rev. Lett.* **76**, 3408 (1996); P. Le Doussal and T. Giamarchi, *Phys. Rev. B* **57**, 11356 (1998).

⁴⁶ Pardo F., de la Cruz F., Gammel P. L., Bucher E., and Bishop D. J., *Nature (London)* **396**, 348 (1998).

⁴⁷ Q.-H. Chen and X. Hu, *Phys. Rev. Lett.* **90**, 117005 (2003).

⁴⁸ J. Lidmar, *Phys. Rev. Lett.* **91**, 097001 (2003).

⁴⁹ U. Divakar, A. J. Drew, S. L. Lee, R. Gilardi, J. Mesot, F. Y. Ogrin, D. Charalambous, E. M. Forgan, G. I. Menon, N. Momono, M. Oda, C. D. Dewhurst, and C. Baines, *Phys. Rev. Lett.* **92**, 237004 (2004).

⁵⁰ M. B. Gaifullin, Y. Matsuda, N. Chikumoto, J. Shimoymaya, and K. Kishio, *Phys. Rev. Lett.* **84**, 2945 (2000).

⁵¹ H. Beidenkopf, N. Avraham, Y. Myasoedov, H. Shtrikman, E. Zeldov, B. Rosenstein, E. H. Brandt, and T. Tamegai, *Phys. Rev. Lett.* **95**, 257004 (2005); H. Beidenkopf, T. Veredene, Y. Myasoedov, H. Shtrikman, E. Zeldov, B. Rosenstein, D. Li, and T. Tamegai, *Phys. Rev. Lett.* **98**, 167004 (2007).

⁵² D. O. G. Heron, S. J. Ray, S. J. Lister, C. M. Aegerter, H. Keller, P. H. Kes, G. I. Menon, and S. L. Lee, *Phys. Rev. Lett.* **110**, 107004 (2013).

⁵³ M. P. A. Fisher, P. B. Weichman, G. Grinstein, and D. S. Fisher, *Phys. Rev. B* **40**, 546 (1989).

⁵⁴ H. Dai, S. Yoon, J. Liu, R. C. Budhani, and C. M. Lieber, *Science* **265**, 1552 (1994).

⁵⁵ U. C. Täuber, H. Dai, D. R. Nelson, and C. M. Lieber, *Phys. Rev. Lett.* **74**, 5132 (1995); D. R. Nelson, *Physica C* **263**, 12 (1996).

⁵⁶ U. C. Täuber and D. R. Nelson, *Phys. Rep.* **289**, 157 (1997); *Phys. Rep.* **296**, 337 (1998).

⁵⁷ L. Radzihovsky, *Phys. Rev. Lett.* **74**, 4923 (1995).

⁵⁸ U. C. Täuber and D. R. Nelson, *Phys. Rev. B* **52**, 16106 (1995); C. Wengel and U. C. Täuber, *Phys. Rev. B* **58**, 6565 (1998).

⁵⁹ A. I. Larkin and V. M. Vinokur, *Phys. Rev. Lett.* **75**, 4666 (1995).

⁶⁰ A. Nandgaonkar, D. G. Kanhere, and N. Trivedi, *Phys. Rev. B* **66**, 104527 (2002).

⁶¹ C. J. van der Beek, M. Konczykowski, V. M. Vinokur, G. W. Crabtree, T. W. Li, and P. H. Kes, *Phys. Rev. B* **51**, 15492 (1995).

⁶² C. J. van der Beek, M. Konczykowski, A. V. Samoilov, N. Chikumoto, S. Bouffard, and M. V. Feigel'man, *Phys. Rev. Lett.* **86**, 5136 (2001).

⁶³ J. C. Soret, V. T. Phuoc, L. Ammor, A. Ruyter, R. De Sousa, E. Olive, G. Villard, A. Wahl, and C. Simon, *Phys. Rev. B* **61**, 9800 (2000).

⁶⁴ J. Lidmar and M. Wallin, *Europhys. Lett.* **47**, 494 (1999).

⁶⁵ L. M. Queiroz, M. D. Coutinho-Filho, and E. P. Raposo, *Eur. Phys. J. B* **88**, 16 (2015).

⁶⁶ C. Dasgupta and O. T. Valls, *Phys. Rev. Lett.* **91**, 127002 (2003); *Phys. Rev. B* **69**, 214520 (2004).

⁶⁷ C. Dasgupta and O. T. Valls, *Phys. Rev. B* **72**, 094501 (2005).

⁶⁸ C. Dasgupta and O. T. Valls, *Phys. Rev. B* **80**, 094517 (2009).

⁶⁹ Y. Nonomura and X. Hu, *Europhys. Lett.* **65**, 533 (2004).

⁷⁰ S. Tyagi and Y. Y. Goldschmidt, *Phys. Rev. B* **67**, 214501 (2003).

⁷¹ S. S. Banerjee, A. Soibel, Y. Myasoedov, M. Rappaport, E. Zeldov, M. Menghini, Y. Fasano, F. de la Cruz, C. J. van der Beek, M. Konczykowski, and T. Tamegai, *Phys. Rev. Lett.* **90**, 087004 (2003); M. Menghini, Y. Fasano, F. de la Cruz, S. S. Banerjee, Y. Myasoedov, E. Zeldov, C. J. van der Beek, M. Konczykowski, and T. Tamegai, *Phys. Rev. Lett.* **90**, 147001 (2003); S. S. Banerjee, S. Goldberg, A. Soibel, Y. Myasoedov, M. Rappaport, E. Zeldov, F. de la Cruz, C. J. van der Beek, M. Konczykowski, T. Tamegai, and V. M. Vinokur, *Phys. Rev. Lett.* **93**, 097002 (2004).

⁷² N. Avraham, Y. Y. Goldschmidt, J. T. Liu, Y. Myasoedov, M. Rappaport, E. Zeldov, C. J. van der Beek, M. Konczykowski, and T. Tamegai, *Phys. Rev. Lett.* **99**, 087001 (2007).

⁷³ A. V. Lopatin and V. M. Vinokur, *Phys. Rev. Lett.* **92**, 067008 (2004); J. Kierfeld and V. M. Vinokur, *Phys. Rev. Lett.* **94**, 077005 (2005).

⁷⁴ Y. Y. Goldschmidt and E. Cuansing, *Phys. Rev. Lett.* **95**, 177004 (2005); Y. Y. Goldschmidt and J.-T. Liu, *Phys. Rev. B* **76**, 174508 (2007).

⁷⁵ L. P. Viana, E. P. Raposo, and M. D. Coutinho-Filho, *Physica C* **437-438**, 341 (2006).

⁷⁶ M. Tinkham, *Introduction to Superconductivity* (Dover, 2004).

⁷⁷ S. J. Chapman, Q. Du, and M. D. Gunzburger, *J. Appl. Math.* **55**, 156 (1995).

⁷⁸ L. N. Bulaevskii, M. Ledvij, and V. G. Kogan, *Phys. Rev. B* **46**, 366 (1992).

⁷⁹ H. E. Stanley, *Introduction to Phase Transitions and Critical Phenomena* (Oxford University Press, 1987).